In Vivo Recognition of Human Vascular Endothelial Growth Factor by Molecularly Imprinted Polymers

Cecchini, Alessandra; Raffa, Vittoria; Canfarotta, Francesco; Signore, Giovanni; Piletsky, Sergey; MacDonald, Michael; Cuschieri, Alfred

Published in:
Nano Letters

DOI:
10.1021/acs.nanolett.6b05052

Publication date:
2017

Document Version
Peer reviewed version

In Vivo Recognition of Human Vascular Endothelial Growth Factor by Molecularly Imprinted Polymers

Alessandra Cecchini[@], Vittoria Raffa[@#], Francesco Canfarotta[$], Giovanni Signore[%+], Sergey Piletsky[^], Michael P. MacDonald[&] and Alfred Cuschieri*[@]*

[@]IMSaT, University of Dundee, 1 Wurzburg Loan, Dundee DD2 1FD, UK

[#]Department of Cellular and Developmental Biology, Università di Pisa, S.S. 12 Abetone e Brennero 4, 56127 Pisa, Italy

[$]MIP Diagnostics Ltd, University Road, Leicester LE1 7RH, UK

[%]Center for Nanotechnology Innovation @NEST, Istituto Italiano di Tecnologia, Piazza San Silvestro 12, 56127 Pisa, Italy

[+]NEST, Scuola Normale Superiore, and Istituto Nanoscienze-CNR, Piazza San Silvestro 12, 56127 Pisa, Italy

[^]Department of Chemistry, University of Leicester, University Road, Leicester LE1 7RH, UK

[&]School of Science and Engineering, University of Dundee, Nethergate, DD1 4HN, UK

IMSaT, University of Dundee, 1 Wurzburg Loan, Dundee DD2 1FD, UK

ABSTRACT One of the mechanisms responsible for cancer-induced increased blood supply in malignant neoplasms is the overexpression of vascular endothelial growth factor (VEGF). Several antibodies for VEGF targeting have been produced for both imaging and therapy.

Molecularly imprinted polymer nanoparticles, nanoMIPs, however, offer significant advantages over antibodies, in particular in relations to improved stability, speed of design, cost and control over functionalization. In the present study, the successful production of nanoMIPs against human VEGF is reported for the first time. NanoMIPs were coupled with quantum dots (QDs) for cancer imaging. The composite nanoparticles exhibited specific homing towards human melanoma cell xenografts, overexpressing hVEGF, in zebrafish embryos. No evidence of this accumulation was observed in control organisms. These results indicate that nanoMIPs are promising materials which can be considered for advancing molecular oncological research, in particular when antibodies are less desirable due to their immunogenicity or long production time.

KEYWORDS molecularly imprinted polymers, composite nanoparticles, zebrafish embryos, cancer imaging, human vascular endothelial growth factor

Angiogenesis is a physiological process concerned with the formation of new blood vessels, essential for sustained viability and growth of malignant solid tumors[1]. This process ensures an adequate blood supply required by various intracellular machineries within cancer cells, e.g. systems driving RNA and protein synthesis, intracellular transport, abnormal tumor-specific metabolic pathways, organelles integrity preservation, etc. Many of the mechanisms involved in these processes remain unresolved, but should become amenable to investigation by molecular-oncological studies carried out by exploiting nanoMIPs. In particular, nanoMIPs, which possess antibody-like properties, are able to cross the cell membrane. Hence, they bear significant potential in accelerating the development of drugs which targets cellular machineries involved in growth and spread of tumor cells, in sharp contrast to conventional chemotherapy agents, which aim to target tumor DNA. Anti-cancer machinery drugs based on this alternative approach to

anti-cancer therapy have been reviewed recently[2]. Amongst the effectors involved in angiogenesis, vascular endothelial growth factor (VEGF) stands out as being the most intensively investigated over the years for its crucial role in this process, both in health and disease[3,4]. Indeed, VEGF is overexpressed in many invasive cancers (breast, colorectal, gastrointestinal, etc.)[5].Through its autocrine secretory activity, it stimulates proliferation of tumor cells together with proliferation and differentiation of endothelial cells[3]. Targeting of VEGF by monoclonal antibodies (mAbs) has been proposed for imaging and detection of the tumor mass[6,7,8]. Additionally, this strategy has been widely exploited for the treatment of several cancers, usually in combination with cytotoxic agents, and it is showing promising results in clinical phase I and phase II with certain cancers[5]. Examples of anti-VEGF antibodies in clinical use or in clinical trial are 2C3, r84, VEGF-trap and particularly Bevacizumab[9]. However, the research in angiogenesis continues with hundreds of groups worldwide developing new ligands, such as aptamers, and new anti-VEGF treatment procedures[10]. There are numbers of issues that remain unresolved in relations to the use of antibodies in research, diagnostics and clinical practice. For instance, production of mAbs is a long, complex and expensive process. Poor cell membrane permeability and possible immunogenic reactions often limit their therapeutic application[11]. Even humanized mAbs can elicit immune reactions[12,13,14] and many have serious, sometimes fatal consequences, e.g., severe neutropenia[15]. Furthermore, functionalization of mAbs with fluorescent reporters or magnetic particles often alter their binding properties. In contrast, the use of molecularly imprinted polymer nanoparticles (nanoMIPs) as molecular active targeting tools has the potential to avert these complications. Molecular imprinting has been extensively exploited for various applications from analytical chemistry to nanomedicine[16]. Recently, a novel approach for the production of nanoMIPs, i.e. solid-phase molecular

imprinting, has been developed leading to the production of MIPs with antibody-like affinity for small drugs, peptides and entire proteins[17]. The increasing interest in employing nanoMIPs for biological applications in preference to antibodies is due to their remarkable properties, e.g., high stability and long shelf life, short development time and low production cost, high affinity and specificity as well as ease of functionalization. NanoMIPs have been utilized as innovative recognition ligands and active targeting tools for the imaging of key molecules, either *in vitro* or *in vivo*[18,19,20,21,22,23]. For example, nanoMIPs have been imprinted against molecules overexpressed on the cell surface[24,25]. In this article, we demonstrate for the first time the successful imprinting of the secreted effector of angiogenesis, human VEGF (hVEGF), which has been proven to play a pivotal role in many invasive cancers and types of leukemia. NanoMIPs targeting hVEGF were produced by solid-phase synthesis and coupled to quantum dots (QDs) to enable fluorescent imaging *in vivo*. Their ability to specifically target hVEGF and homing towards the tumor mass was confirmed in xenotransplantation of human malignant melanoma cells in zebrafish embryos[26]. These new highly fluorescent nanoMIPs can be used for the study of angiogenesis as well as potential imaging tools in cancer diagnostics.

For this study, a synthetic nine-aminoacid surface epitope of hVEGF (amino acids 83–91: IKPHQGQHI) (Figure 1c) was selected as template for the solid-phase synthesis of nanoMIPs against hVEGF. The epitope choice was dictated by specific criteria including: (i) compatibility with the molecular imprinting technology (i.e. short epitope); (ii) possibility to add a terminal cysteine for the immobilization onto the solid phase; (iii) accessibility (i.e. surface epitope) (Figure 1a – b); (iv) relevance of the sequence of the epitope (i.e. specific of hVEGF and in the receptor recognition region of hVEGF). The epitope was selected after literature research[27],

modified with a terminal cysteine (final sequence: IKPHQGQHI–C), and immobilized onto micrometric glass beads for the subsequent solid-phase synthesis of anti-hVEGF nanoMIPs.

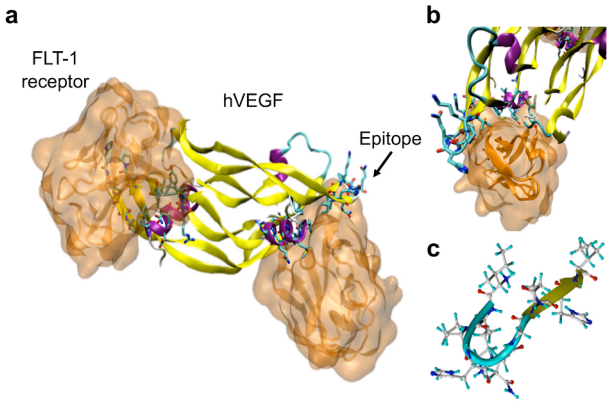

Figure 1. The structure of human vascular endothelial growth factor (hVEGF) and the selected epitope, in complex with VEGF receptor FLT-1. (a) Virtual image of hVEGF associated to its receptor FLT-1 and the position of the chosen epitope for the solid-phase synthesis. (b) Rotated virtual image of hVEGF associated to its receptor FLT-1; it is possible to better observe from a different angle the position of the epitope in the whole sequence in the recognition site of the receptor. (c) The selected nine-aminoacid epitope of hVEGF (IKPHQGQHI) isolated from the whole sequence.

We elected to couple the recognition property of nanoMIPs with high brightness and high-photostability 710 nm emitting CdTe QDs, as NIR emission can be exploited to perform *in vivo* imaging with high spatial resolution, deep tissue penetration and low auto-fluorescence. We adopted two different approaches to generate the final fluorescent hybrid nanoprobe – QD-MIPs. One approach was based on the incorporation of commercial carboxyl-functionalized QDs into the MIP matrix (i.e. within the nanoMIPs) during the polymerization process (Figure 2a) – QD-

MIPs (embedded). This was achieved by previous functionalization of the QDs with the functional monomer N-(3-aminopropyl) methacrylamide. Although QDs were successfully embedded within MIP matrix (Figure 2c), QD-MIPs obtained by this approach did not exhibit any fluorescence signal, probably because of quenching events following the polymerization process. The other strategy aimed to covalently couple the QDs onto the MIP surface after the polymerization process (Figure 2a) – QD-MIPs (attached). TEM images of QD-MIPs (attached) revealed the successful attachment of QDs onto the surface of pre-synthesized MIPs (Figure 2d). QD-MIPs showed an emission peak at 730 nm; shifted 20 nm towards infrared when compared to free QDs (Figure 2e). This shift was previously encountered for QDs functionalized with monomer N-(3-aminopropyl) methacrylamide, exploited in the first approach. Though the precise mechanism for this shift in the emission peak is not known, it is to be expected due to the close coupling of the QDs to the monomers[28]. Control polymers imprinted against non-target vancomycin were also coupled to QDs following the second approach. Similarly, the obtained control nanoprobes – QD-nips – were observed to bear fluorescence after the functionalization (Figure S2a). QD-MIPs were characterized in terms of size, affinity and specificity for the template, and their ability to bind the entire protein hVEGF. Dynamic light scattering measurements confirmed the production of QD-MIPs with 171.4 ± 36.3 nm hydrodynamic diameter (Figure 2f), whereas QD-nips show diameter of 140.2 ± 16 nm (Figure S2b)[29]. Additionally, we performed nanoparticle tracking analysis (NTA) on hybrid nanoprobes and non-functionalized MIPs. Particularly, QD-MIPs showed diameter of 140.0 ± 6.8 nm, whereas MIPs 120.6 ± 10.5 nm diameter (Figure S1, Table S3). As expected, NTA measurement provided slightly smaller values than the ones detected with DLS, since DLS measures the light scattered from each nanoparticle in the sample as a whole, giving an average measurement. Z

potential measurements showed a shift of the surface charge of QD-MIPs (attached) (-11.9 ± 0.8 mV) from the value of non-functionalized MIPs (-27.5 ± 4.8 mV) to the less negative value obtained for free QD (-3.76 ± 2.0 mV), confirming the presence of QDs onto the surface of nanoMIPs (Figure S1, Table S3). Conversely, QD-MIPs (embedded) were found to present similar surface charge to non-functionalized MIPs (Table S1).

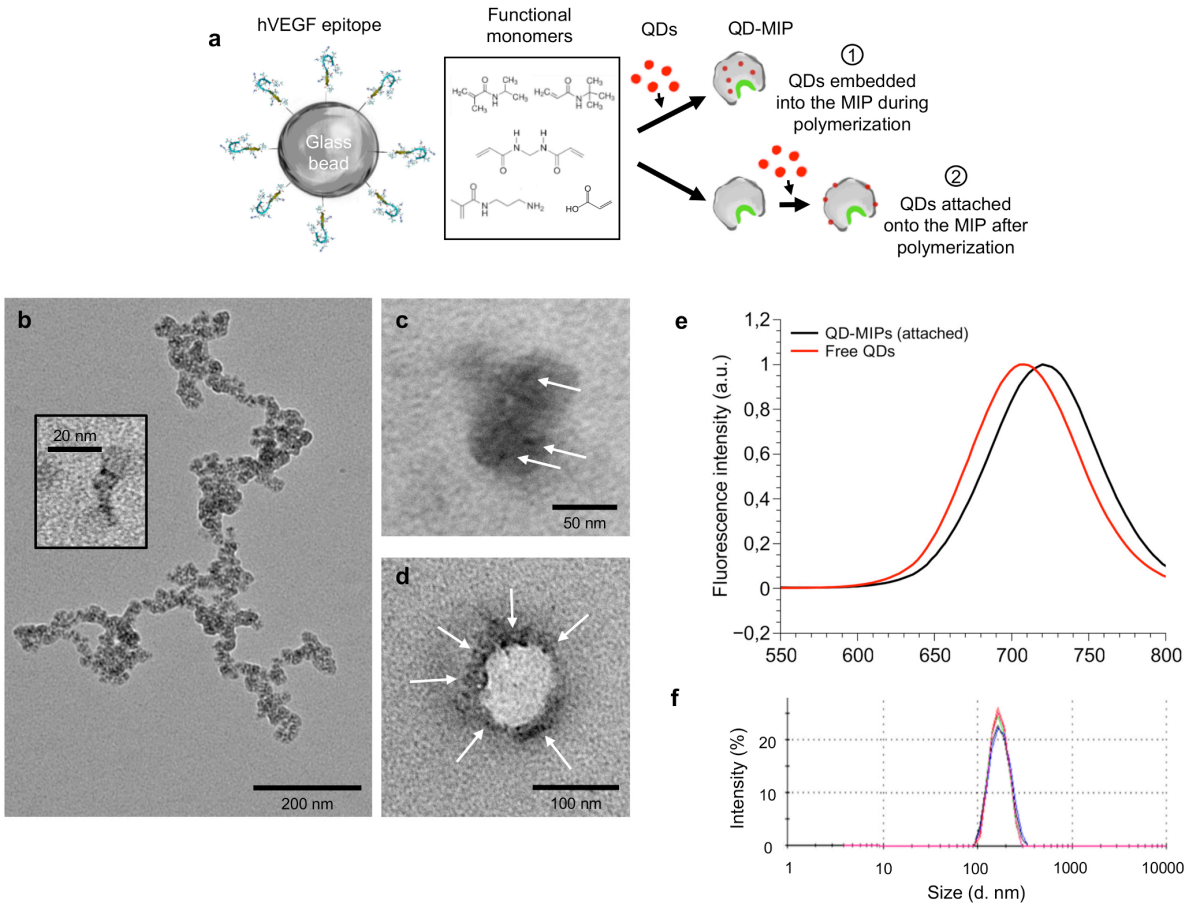

Figure 2. Scheme of the polymerization approach and the strategy to produce the QD-MIP nanoprobes, together with TEM images, fluorescence and size measurements. (a) Cartoon of the two strategies exploited to produce QD-MIPs, based on solid-phase synthesis: (i) embedding the QDs in the MIP matrix during its polymerization; (ii) attaching the QDs onto the nanoMIPs after the polymerization process. TEM images of (b) QDs which appear as electron-dense spots 2-4

nm in size (inset), (c) MIP with incorporated electron-dense QDs in the matrix (arrows) – QD-MIP (embedded), (d) MIP exhibiting a surface decorated with electron-dense QDs (arrows) – QD-MIP (attached). (e) Fluorescence profile of QD-MIPs with QDs embedded into the MIPs during the polymerization - QD-MIPs (embedded) -, QD-MIPs with QDs attached via EDC/NHS onto the nanoMIPs surface after the polymerization step – QD-MIPs (attached) -, and free QDs (Graph obtained with Qti-plot). (f) Dynamic light scattering measurements of fluorescent QD-MIPs polymerized in PBS against the epitope of hVEGF with hydrodynamic diameter 171.4 ± 36.3 nm (n=6).

The affinity of QD-MIPs imprinted against the epitope of hVEGF was assessed using a surface plasmon resonance (SPR) instrument (Biacore 3000). In particular, QD-MIPs were covalently immobilized on the sensor surface and increasing concentrations of the epitope were injected. QD-MIPs showed an excellent affinity for the epitope, with K_D in the low nanomolar range (1.56 ± 0.20 nM) and low Chi^2 values (Table S1, Figure 3a). Similarly, QD-MIPs were also able to bind the whole hVEGF protein. The graph in Figure 3b shows the binding and dissociation curves after the injection of 40 nM recombinant hVEGF. Furthermore, the binding is highly specific, as exemplified by SPR measurements which demonstrated absence of binding of QD-MIPs to a non-target molecule. We decided to focus our attention on a molecule similar in terms of isoelectric point to our whole-sequence target hVEGF (8.5) and cysteine-epitope (8.14); for which we chose the antibiotic vancomycin (8.14). This molecule was not recognized by QD-MIPs even at concentrations up to 1 μM (three orders of magnitude higher than the ones used for hVEGF) (Figure 3b – c).

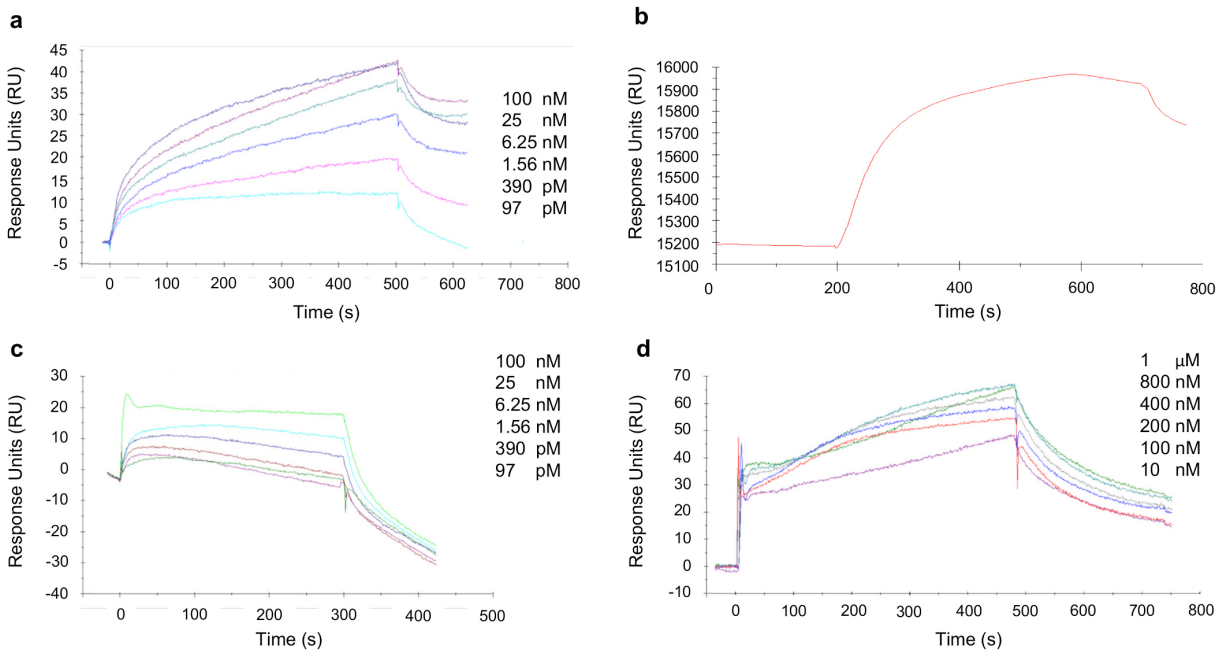

Figure 3. Surface plasmon resonance measurements obtained with a Biacore 3000 instrument (GE Healthcare). (a) Binding curves of QD-MIPs imprinted against the epitope of hVEGF and tested for the epitope. For the calculation of the affinity for the epitope, 6 different concentrations of the epitope (ranging from 97 pM to 100 nM) were injected on the QD-MIP functionalized gold chip exploited for the analysis. (b) Binding assessment of the QD-MIPs for the whole protein hVEGF (concentration injected 40 nM). (c) Binding curves of QD-MIPs imprinted against the epitope of hVEGF after injection of 6 different concentrations of the non-target vancomycin (97 pM – 100 nM), for assessing the specificity of QD-MIPs for the epitope. (d) Binding curves of QD-MIPs after injection of 6 different concentrations of the non-target vancomycin (10 nM – 1 μM), for assessing the specificity of QD-MIPs for the epitope. Experiments n= 2.

SPR measurements were also performed using an epitope of the epidermal growth factor receptor (EGFR) as control protein. Interestingly, EGFR is endogenously produced in zebrafish[30] and it is known to be involved in angiogenesis, therefore it could be one of the proteins exposed to QD-MIPs in xenotransplanted zebrafish embryos. Concentrations of EGFR epitope ranging from 97 pM to 100 nM (as per hVEGF epitope and vancomycin) were injected (Figure S). The goodness of the fit of data obtained from Biacore measurements was poor and therefore it did not allow calculating any K_D, which resulted in the confirmation of specificity of our hybrid nanoprobes for hVEGF template.

SPR measurements allowed us to conclude that QD-MIPs imprinted against hVEGF had high affinity and specificity for the epitope and were able to bind the whole hVEGF.

The next step in our experiments was to assess the ability of QD-MIPs to localize *in vivo*, namely in tumor xenografts in zebrafish embryos. Specifically, a melanoma cell line known to overexpress hVEGF was exploited to create the *in vivo* model. Zebrafish embryos were selected as animal model for this study for several reasons: (i) 'casper' transgenic fish are transparent; (ii) their maintenance and manipulation are straightforward; (iii) they develop quickly compared to mice; (iv) zebrafish are a widely used model in studies of human tumors; (vi) they can be used at unlicensed development stages, within the temporal window between the fecundation and 96 hours post fertilization (hpf) (rejection-free xenografts)[31]. Two tumor models were obtained by injecting two human melanoma cell lines in the yolk of 48 hpf zebrafish embryos: (i) WM-266, overexpressing hVEGF (called hVEGF (+) model hereafter) and (ii) A-375, with low expression of hVEGF (called hVEGF (-) model hereafter)[32,33]. Targeted and non-targeted nanoMIPs (i.e., nanoMIPs imprinted against vancomycin, QD-nips hereafter) were administered 24 hours after the injection of the tumor cells. Specifically, QD-MIPs were injected in both the hVEGF (-) and

the hVEGF (+) models, whereas QD-nips were administered only to the hVEGF (+) model (Figure 4a). Initially, we performed a study on the toxicity of these hybrid nanoprobes in zebrafish embryos. The effect of QD-MIP injection in the animals was evaluated. Any toxic effects should result in reduced viability and/or alterations of normal development. The most common phenotype mutations caused by nanoparticles in zebrafish embryos include intestinal defects, tail or spinal cord flexure, fin-fold abnormalities, yolk sac edema, absence of tail, twisted notochord, pericardial edema, degeneration of body parts, jaw defects, head skeleton defects, neurological damage and anencephaly[31]. QD-MIPs were injected in the yolk of 48 hpf zebrafish embryos. Twenty-four hours post-injection, the embryos were imaged and dead or aberrant phenotypes were recorded. Data analysis showed no statistically significant difference between groups ($n=40$, $p>0.5$, Chi2 test) (Figure S). We can conclude that, for the purpose of this study, QD-MIPs induce negligible toxic effects. Prior to start experiments of QD-MIP homing towards the tumor, we sought to find the most appropriate incubation time to allow efficient diffusion without incurring loss of the fluorescent reporter. To this end, 48 hpf zebrafish embryos were injected with QD-MIPs and then sacrificed at different incubation times: time 0, 2.5 hours and overnight (20 hours). Thereafter, embryos were digested and their cadmium content, a marker of QD-MIPs concentration, was analyzed by inductively coupled plasma mass spectrometry. The results showed significant decrease in cadmium concentration down to 57% in the 2.5-hour incubation sample, compared to time 0 incubation. Cadmium signal was even lower in overnight incubation sample (36%) compared to time 0 (Table S2). Based on these findings, we incubated the nanoprobes for 7 hours in either hVEGF (+) or hVEGF (-) zebrafish models. This time was selected as a reasonable compromise between the long interval necessary to allow diffusion of nanoprobes in the yolk of zebrafish embryos and fluorescence signal loss. Confocal

microscopy was used to detect the *in vivo* distribution of injected nanoprobes and to compare it with the tumor mass localization. Considering the nature of hVEGF as secreted effector of angiogenesis, we did not expect to observe co-localization of the QD-MIPs with WM-266 cells, but mostly homing of the nanoprobes towards cancer cells. Notably, Figure 4b shows that QD-MIPs were actually able to home towards the cells in hVEGF (+) model and specifically localize in close proximity to the tumor mass. In contrast, in both controls, QD-MIPs in hVEGF (-) model and QD-nips in hVEGF (+) model, nanoprobes did not localize with the tumor mass (Figure 4b). Importantly, data analysis highlighted a statistically significant difference in the means of the nanoprobe-cell distances between the QD-MIPs injected in hVEGF (+) embryos and the two controls, with p-value= 0.0006 (Figure 4c).

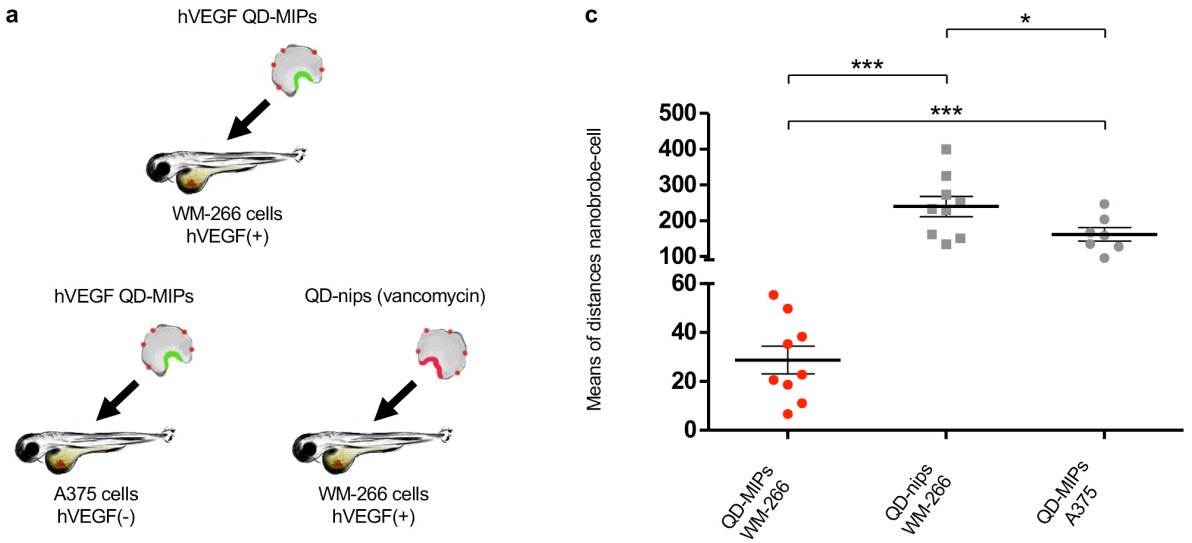

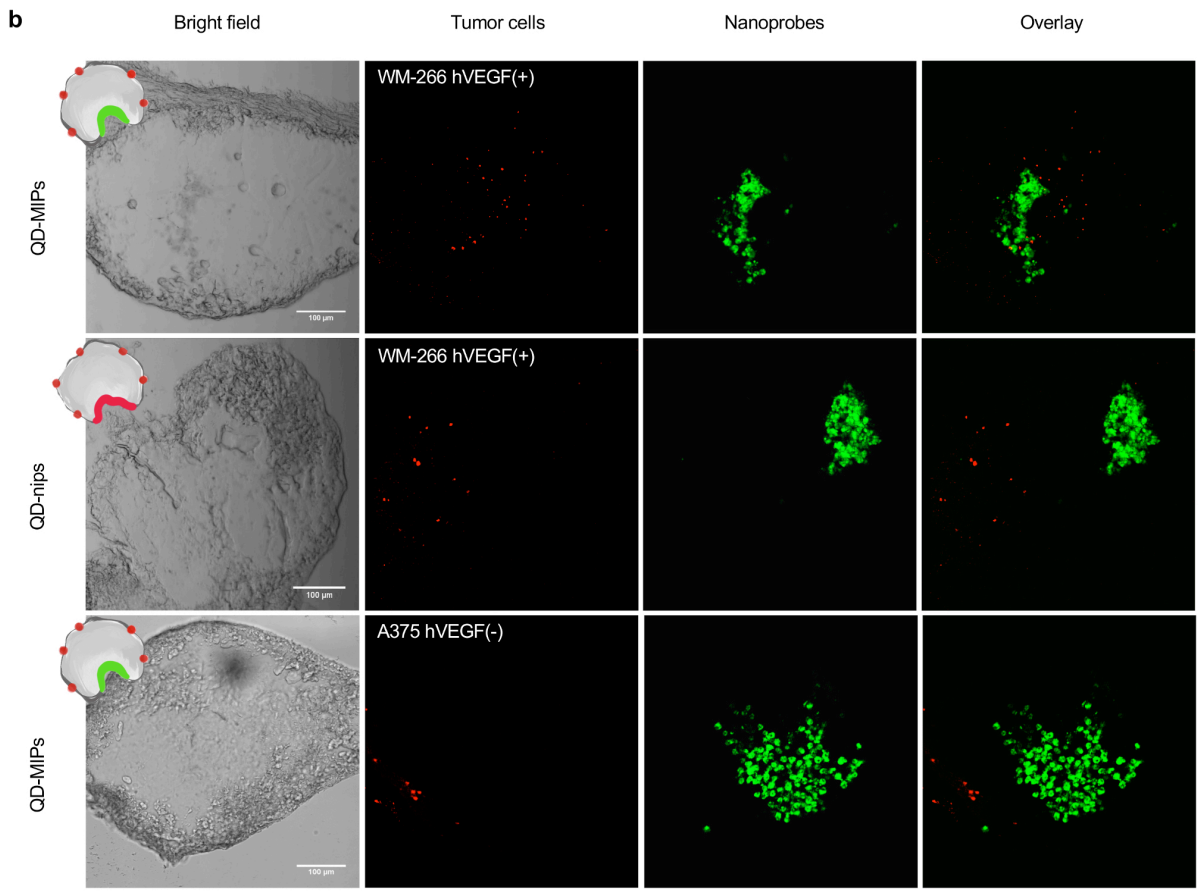

Figure 4. Overview of the *in vivo* experiments carried out exploiting zebrafish embryos to investigate the ability of QD-MIPs to localize with cancer cells overexpressing hVEGF. (a) Scheme of the *in vivo* experiments: (i) QD-MIPs imprinted against hVEGF injected in hVEGF (+) model, (ii) QD-MIPs injected in hVEGF (-) model, (iii) QD-nips imprinted against vancomycin injected in hVEGF (+) model. (b) Panel of the bright field and fluorescence images of human melanoma cells (WM-266 hVEGF (+) model and A-375 hVEGF (-) model) (green) and the fluorescent nanoprobes (red), acquired with a confocal microscope Leica SP2 (scale bar 100μm), and the overlay of the two signal. (c) Statistical analysis of the mean of distances nanoprobe-cell (μm) in the three different scenarios: QD-MIPs injected in hVEGF (+) model, QD-nips injected in WM-266 hVEGF (+) model, and QD-MIPs injected in hVEGF (-) model. ANOVA Bonferroni was performed showing p-value= 0.0006. Embryos n≥ 7.

In the present study, we demonstrate that QD-MIP hybrid nanoprobes, emitting in the near-infrared and imprinted against the surface epitope of hVEGF, recognize and selectively bind to the entire protein *in vitro*, and home towards the tumor mass overexpressing hVEGF in *in vivo* tumor xenograft experiments. Here, we demonstrate for the first time that a secreted factor has been successfully targeted using MIP-based composite nanoparticles. Hence, these findings indicate the significant potential of nanoMIPs, paving the way for additional studies to target other secreted factors in several human disorders. We also conclude that nanoMIPs may represent a viable alternative to conventional active targeting ligands such as monoclonal antibodies. The main advantages of MIPs as compared with mAbs are related to their rapidity of development (3 days for synthesis and functionalization of nanoMIPs), long shelf-life, easy functionalization, good biocompatibility, solubility and ability to cross the cell membrane and lack of immunogenic response[34]. The versatility of the solid-phase synthesis approach should permit the coupling of nanoMIPs with multiple fluorescent reporters or cargos. Magnetic nanoparticles would have to be considered as contrast agents for magnetic resonance imaging for clinical translation of this strategy, or Cd-free QDs, especially in view of the advances in their composition and increased biocompatibility in recent years. By virtue of their ease of functionalization, nanoMIPs could be conjugated to various drugs for non-invasive detection of early subclinical cancer and simultaneous drug therapy. Additionally, since the epitope exploited as a template for solid-phase polymerization is strongly involved in the recognition of the hVEGF receptor, these nanoprobes may exhibit antagonist properties as anti-VEGF therapeutic agents, and therefore its angiogenetic cascade. Experiments are currently being planned in our lab to generate novel nanoprobes having combined diagnostic and therapeutic properties.

ASSOCIATED CONTENT

Supporting Information

Experimental methods for the preparation of QD-MIPs and *in vivo* experiments and techniques exploited for the characterization of QD-MIPs and investigation of their behavior *in vitro* and *in vivo* (.PDF).

Supplementary figures and tables for size and z potential measurements, characterization of control hybrid nanoparticles QD-nips for fluorescence and size, zebrafish injection and production of the two models, data acquisition and imaging analysis, and data of SPR, ICP-MS measurements, NTA, and z potential (.PDF).

Table of Contents (.TIF).

Corresponding Author

Vittoria Raffa v.s.raffa@dundee.ac.uk; Alfred Cuschieri a.cuschieri@dundee.ac.uk

Author Contributions

A.C. prepared and characterized the nanoprobes *in vitro* and performed the *in vivo* experiments and confocal microscopy. A.C. wrote the paper. V.R., F.C., G.S. contributed to the experimental activities and to edit the manuscript. All authors discussed the results, contributed to data analysis, and commented on the manuscript. S.P. and A.Cu. designed the experiments and supervised the research.

Funding Sources

The research leading to these results has received funding from the People Programme (Marie Curie Actions) of the European's Seventh Framework Programme (FP7/2007-2013) under REA grant agreement no. 608133.

ACKNOWLEDGMENT

The research leading to these results has received funding from the People Programme (Marie Curie Actions) of the European's Seventh Framework Programme (FP7/2007-2013) under REA grant agreement no. 608133. The authors acknowledge Matteo Battaglini, Martina Giannaccini, and Luciana Dente for the assistance for *in vivo* experiments in zebrafish and their valuable insights; Kalhum Karim and Antonio Guerreiro for the training in SPR measurements and evaluation; David Porciani for the suggestions for functionalization of the nanoprobes and the helpful discussions; Kurt Ballmer for providing recombinant hVEGF. The authors also thank Paolo Lucchesi and Franco Verni for the TEM analysis performed at CIME (Centro Interdipartimentale di Microscopia Elettronica), Università di Pisa (Italy).

F.C and S. P. declare competing financial interests.

REFERENCES

(1) Ferrara, N. *Nat. Rev. Cancer* **2002,** *2,* 795–803.

(2) Dobbelstein, M.; Moll, U. *Nat. Rev. Drug Discov.* **2014,** *13,* 179–96.

(3) Ellis, L. M.; Hicklin, D. J. *Nat. Rev. Cancer* **2008,** *8,* 579–91.

(4) Goel, H. L.; Mercurio, A. M. *Nat. Rev. Cancer* **2013,** *13,* 871–82.

(5) Reinacher-Schick, A.; Pohl, M.; Schmiegel, W. *Nat. Clin. Pract. Gastroenterol. Hepatol.* **2008,** *5,* 250–267.

(6) Foersch, S.; Kiesslich, R.; Waldner, M. J.; Delaney, P.; Galle, P. R.; Neurath, M. F.; Goetz, M. *Gut* **2010,** *59,* 1046–55.

(7) Choi, Y. E.; Kwak, J. W.; Park, J. W. *Sensors* **2010,** *10,* 428–455.

(8) Pan, L. H.; Kuo, S. H.; Lin, T. Y.; Lin, C. W.; Fang, P. Y.; Yang, H. W. *Biosens. Bioelectron.* **2016,** *89,* 598–605.

(9) Sullivan, L. A.; Brekken, R. A. *MAbs* **2010,** *2,* 165–175.

(10) Jain, R. K.; Duda, D. G.; Clark, J. W.; Loeffler, J. S. *Nat. Cilin Pract. Oncol* **2006,** *3,* 24–40.

(11) Buelow, R.; Platzer, J.; van Schooten, J.; Buelow, J. U. *US 7129084 B2*, **2003**, 0–4.

(12) Ecker, D. M.; Jones, S. D.; Levine, H. L. *MAbs* **2015,** *7,* 9–14.

(13) Berg, T. *Angew. Chem. Int. Ed. Engl.* **2003,** *42,* 2462-2481.

(14) Gadek, T. R.; Nicholas, J. B. *Biochem. Pharmacol.* **2003,** *65,* 1–8.

(15) Hansel, T. T.; Kropshofer, H.; Singer, T.; Mitchell, J. A.; George, A. J. T. *Nat. Rev. Drug Discov.* **2010,** *9,* 325–338.

(16) Piletsky, S. A.; Turner, N. W.; Laitenberger, P. *Med. Eng. Phys.* **2006,** *28,* 971–7.

(17) Mosbach, K.; Ramström, O. *Nat. Biotechnol.* **1996,** *14,* 163-170.

(18) Rostamizadeh, K.; Vahedpour, M.; Bozorgi, S. *Int. J. Pharm.* **2012,** *424,* 67–75.

(19) Basozabal, I.; Guerreiro, A.; Gomez-Caballero, A.; Aranzazu Goicolea, M.; Barrio, R. J. *Biosens. Bioelectron.* **2014,** *58,* 138–144.

(20) Shutov, R. V.; Guerreiro, A.; Moczko, E.; De Vargas-Sansalvador, I. P.; Chianella, I.; Whitcombe, M. J.; Piletsky, S. A. *Small* **2014,** *10,* 1086–1089.

(21) Abdin, M. J.; Altintas, Z.; Tothill, I. E. *Biosens. Bioelectron.* **2015,** *67,* 177–183.

(22) Zeng, Z.; Hoshino, Y.; Rodriguez, A.; Yoo, H.; Shea, K. J. *ACS Nano* **2010,** *4,* 199–204.

(23) Hoshino, Y.; Koide, H.; Urakami, T.; Kanazawa, H.; Kodama, T.; Oku, N.; Shea, K. J. *JACS* **2010,** *132,* 6644–6645.

(24) Yin, D.; Wang, S.; He, Y.; Liu, J.; Zhou, M.; Ouyang, J.; Liu, B.; Chen, H. Y.; Liu, Z.

Chem. Commun. (Camb). **2015,** *51,* 17696–17699.

(25) Kunath, S.; Panagiotopoulou, M.; Maximilien, J.; Marchyk, N.; Sänger, J.; Haupt, K. *Adv. Healthc. Mater.* **2015,** *4,* 1322–1326.

(26) White, R.; Rose, K.; Zon, L. *Nat. Rev. Cancer* **2013,** *13,* 624–36.

(27) Fuh, G.; Wu, P.; Liang, W. C.; Ultsch, M.; Lee, C. V.; Moffat, B.; Wiesmann, C. *J. Biol. Chem.* **2006,** *281,* 6625–6631.

(28) Wang, D.; He, J.; Rosenzweig, N.; Rosenzweig, Z. *Nano Lett.* **2004,** *4,* 3–7.

(29) Canfarotta, F.; Poma, A.; Guerreiro, A.; Piletsky, S. *Nature Protocol*. **2016**, *11*, 443-455.

(30) Goishi, K.; Lee, P.; Davidson, A. J.; Nishi, E.; Zon, L. I.; Klagsbrun, M. *Mechanisms of Development*, **2003**, *120*, 811-822.

(31) Giannaccini, M.; Cuschieri, A.; Dente, L.; Raffa, V. *Nanomedicine Nanotechnology, Biol. Med.* **2014,** *10,* 703–719.

(32) Yang, L.; Chen, G.; Mohanty, S.; Scott, G.; Fazal, F.; Rahman, A.; Begum, S.; Hynes, R. O.; Xu, L. *Cancer Res.* **2011,** *71,* 5558–5568.

(33) Graells, J.; Vinyals, A.; Figueras, A.; Llorens, A.; Moreno, A.; Marcoval, J.; Gonzalez, F. J.; Fabra, A. *J. Invest. Dermatol.* **2004,** *123,* 1151–1161.

(34) Canfarotta, F.; Waters, A.; Sadler, R.; McGill, P.; Guerreiro, A.; Papkovsky, D.; Haupt, K.; Piletsky, S. A. *Nano Res.* **2016,** *9,* 3463-3477.